

Journal of Materials Chemistry B

Accepted Manuscript

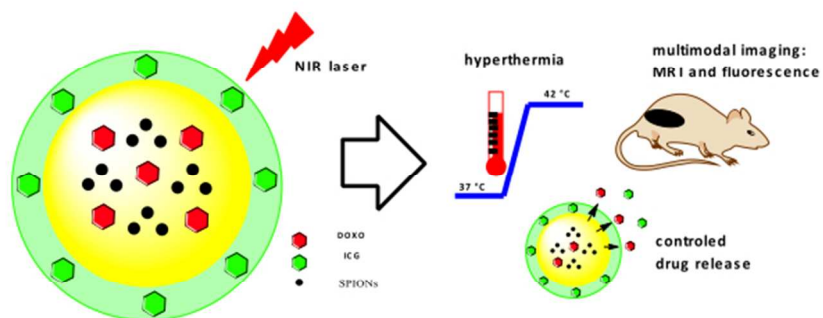


This is an *Accepted Manuscript*, which has been through the Royal Society of Chemistry peer review process and has been accepted for publication.

Accepted Manuscripts are published online shortly after acceptance, before technical editing, formatting and proof reading. Using this free service, authors can make their results available to the community, in citable form, before we publish the edited article. We will replace this *Accepted Manuscript* with the edited and formatted *Advance Article* as soon as it is available.

You can find more information about *Accepted Manuscripts* in the [Information for Authors](#).

Please note that technical editing may introduce minor changes to the text and/or graphics, which may alter content. The journal's standard [Terms & Conditions](#) and the [Ethical guidelines](#) still apply. In no event shall the Royal Society of Chemistry be held responsible for any errors or omissions in this *Accepted Manuscript* or any consequences arising from the use of any information it contains.



Multifunctional hybrid polymeric-based nanoplateforms for simultaneous fluorescence and magnetic resonance imaging and multimodal chemo- and photothermal therapies

254x190mm (72 x 72 DPI)

ARTICLE

NIR-Light Active Hybrid Nanoparticles for Combined Imaging and Bimodal Therapy of Cancerous Cells

Cite this: DOI: 10.1039/x0xx00000x

Received 00th January 2012,
Accepted 00th January 2012

DOI: 10.1039/x0xx00000x

www.rsc.org/

A. Topete,^a D. Melgar,^{a,†} M. Alatorre-Meda,^{a,†} P. Iglesias,^b B. Argibay,^c S. Vidawati,^a S. Barbosa,^{a,*} J. A. Costoya,^b P. Taboada,^{a,*} V. Mosquera,^a

We report the synthesis of a multifunctional biocompatible theranostic nanoplatform consisting of a biodegradable PLGA matrix surface-functionalized with indocyanine green (ICG), a near-IR fluorescent dye, and co-loaded with superparamagnetic iron oxide nanoparticles (SPIONs) and the anticancer drug doxorubicin (DOXO). Combination of chemo- and photothermal therapeutic efficacy as well as magnetic resonance and optical fluorescence imaging performance were successfully tested *in vitro* on a tumoral cervical HeLa cell line. Magnetic *in vitro* guided targeting of these nanoplatforms was also proven. These nanoconstructs also enabled to monitor their *in vivo* biodistribution by fluorescence imaging in a mice model, which revealed their effective accumulation in the tumor and, unexpectedly, in the brain area. A lower presence of nanoplatforms was noted in the reticulo-endothelial system. The present observations suggest the nanoplatforms ability to possibly overcome the blood brain barrier. These results open up new possibilities to use our multifunctional nanoplatforms to treat brain-located diseases.

A Introduction

The advances provided by nanotechnology have offered new opportunities to develop novel nanocarriers able to improve the pharmacokinetics and the local bioavailability of a variety of drugs as well as providing additional functionalities including imaging, diagnosis or targeting with the final objective of obtaining true multifunctional nanomedical platforms in a single nanodevice.¹⁻⁴ These nanoplatforms open new windows to overcome still unresolved impediments in clinical practice, and in particular, in cancer therapeutics, such as the substantial toxicity of required drug doses to completely eliminate tumors; the poor effectiveness of drug treatments against multi-drug resistant cancer cells; the impossibility of early detection of very small tumors or blood circulating malignant cells; or the spatial-temporal separation of diagnosis and therapeutic clinical phases, amongst others.^{2,3}

To construct multifunctional nanoplatforms, biodegradable polymeric nanoparticles (NPs) are an interesting approach provided that they are frequently used to improve the therapeutic impact of different types of drugs and bioactive molecules by enhancing their solubilization, their interaction with the biological environment, their absorption into a selected tissue, their bioavailability, their retention time and intracellular penetration,^{5,6} while simultaneously reducing the risks of toxicity and economical costs. To this end, poly-D,L-lactide-co-glycolide (PLGA) copolymer is one of the most successfully used biodegradable polymers for the development of nano- and micro-particle-based drug delivery systems and scaffolds for tissue engineering^{7,8} provided that it undergoes hydrolysis in the

body to produce biodegradable and biocompatible metabolite monomers, lactic acid and glycolic acid, with the additional advantage of being commercially available in a wide range of molecular weights and compositions. For these reasons, PLGA nanoparticles (PLGA NPs) have been used for the encapsulation of a wide range of active compounds (drugs, vaccines, proteins, or nucleic acids amongst others),⁹ exhibiting a high stability and loading capacity, and offering various feasible routes of administration. These characteristics have led to its approval by the US FDA and European Medicines Agency (EMA) to be used in several drug delivery systems in humans.¹⁰⁻¹²

PLGA NPs were selected in some previous prospective studies to construct new multifunctional systems allowing simultaneous diagnosis and therapy (*e.g.* nanotheranostics devices). For example, the anticancer drug doxorubicin (DOXO) was bound to magnetic NPs that were embedded in a PLGA matrix by means of hydrophobic interactions. DOXO was sustainably released without inhibition due to the presence of the magnetic particles, which additionally provided the ability of magnetically-guided targeting through the application of an external magnetic field.^{13,14} In a similar approach, Yang *et al.*¹⁵ also co-loaded DOXO and superparamagnetic iron oxide NPs (SPIONs) inside PLGA NPs surface-functionalized by a monoclonal antibody (Herceptin, HER) to serve as an active targeting moiety on SK-BR3 cells, which overexpress the human epidermal growth factor receptor-2 (HER2). More recently, Kim *et al.*¹⁶ also synthesized DOXO/SPION or DOXO-quantum dots (QDs) co-loaded PLGA NPs stabilized with a polylysine-PEG-folate polymer to provide the nanoplatform with

simultaneous chemotherapeutic, imaging (magnetic resonance, MRI, or fluorescence optical, FOI, imaging) and active targeting capabilities. Also, SPIONs embedded in PLGA NPs were designed as a dual drug delivery and imaging system able to encapsulate both hydrophilic (carboplatin) and hydrophobic drugs (paclitaxel and rapamycin). Both *in vitro* and *in vivo* MR imaging showed that these NPs possess a better image resolution than commercial contrast agents.^{17,18} Very recently, PLGA NPs incorporating QD, SPIONs and Au NPs were obtained for labelling, imaging and tracking of neutrophils for *in vivo* applications.¹⁹

In this work, we design a magnetically-targeted multifunctional nanoplatform able to be used for simultaneous magnetic resonance and optical imaging and multimodal chemo-/photothermal therapeutic activities. The present nanoplatform offers several advantages in comparison with previous analysed systems such as: the avoidance of complicated chemical synthetic steps to provide the nanosystem with the phototherapeutic activity, as the *in situ* growth of a metal layer done in previous works;^{20,21} its ability to potentially provide simultaneous capabilities for dual imaging (MRI and fluorescence) and/or therapy (chemo- and photothermal activities); and the use of only biocompatible and FDA-approved components. To achieve this, the present nanoplatform is composed of four different components: A PLGA NPs were used as a core matrix for co-loading of DOXO as a chemotherapeutic agent, and hydrophobic SPIONs for both magnetically-guided targeting and T_2 -MRI imaging. Indocyanine green (ICG), a tricyanocyanine dye with light absorbing properties exclusively in the near IR (NIR) region wavelengths and currently used as a diagnostic compound for blood volume determination, ophthalmic angiography, cardiac output and hepatic function,^{22,23} is complexed to the chitosan-functionalized surface of PLGA NPs to provide the system with optical imaging and photo-thermal therapy capabilities under NIR light irradiation. Since these nanoplatforms are NIR-resonant, the simultaneous effect of targeted NIR-induced hyperthermia and chemotherapy results in larger cell toxicities in HeLa cervical and breast MDA-MB-231 cancer cell lines at low drug concentrations, highlighting a synergistic effect. Furthermore, magnetic targeting additionally enhances the therapeutic efficacy of the nanoplatforms.

B Results and Discussion

To design our nanoplatform we first established the optimal physico-chemical properties of the PLGA core matrix provided that factors such as particle size and NP surface properties can influence circulation times, biodistribution, interactions of NPs with cells and tissues and their ability to cross physiological barriers.²⁴ The main aims were to control the PLGA NP size, their surface properties and the cargo release rate, which are influenced by different parameters involved in the NP synthetic procedure, *i.e.* molecular weight and concentration of PLGA chains, nature and concentration of the stabilizing agent, volumes of the oil and aqueous phases and concentrations of cargo molecules, amongst others (see Electronic Supplementary Information for details, Figure S1 and Figure S2). Then, we standardized the preparation of DXSP-PLGA NPs to achieve sufficiently small NP sizes to enable a parenteral NP administration route, avoidance of NP recognition by macrophages, elevated zeta potentials to ensure colloidal stability and high cargo payloads when required (see Experimental Section for details). Hence, we first loaded SPIONs and the chemotherapeutic drug DOXO in the core of PLGA NPs obtained by a modified nanoprecipitation method. The oleic acid-stabilized SPIONs had a mean diameter of ca. 10 nm, and were obtained by a co-precipitation method (Figure S3a). The X-ray diffraction pattern

of the as-synthesized SPIONs clearly indicated that they are formed exclusively by magnetite (Fe_3O_4) (Figure S3b). The SPIONs were uniformly assembled and distributed throughout the PLGA matrix (Figure 1a). This might result from i) hydrophobic interactions between the oleic acid chains stabilizing SPIONs, drug molecules, and PLGA chains; ii) hydrogen bonding between functional groups of the surfactant and polymeric chains, and/or iii) to existing dipole-dipole interactions between the entrapped SPIONs. The size of DXSP-PLGA NPs was estimated to be ca. 122 ± 11 nm by DLS, with a surface electric charge of -35.3 ± 4.8 mV, which seems to be suitable for NPs passive tumor targeting through the enhanced permeability and retention effect (EPR).²⁵ The successful incorporation of DOXO inside the hybrid NPs was corroborated by the appearance of absorption and fluorescence emission peaks at ca. 480 and 591 nm, respectively, consistent with the spectra of free DOXO (Figure 1b and Figure S4). The lower DOXO fluorescence in the NPs if compared to that of an equivalent amount of free DOXO stems from the self-quenching effect of the drug inside the polymeric matrix.²⁶

After coating PLGA NP surfaces with LMW-chitosan, the estimated size of the hybrid NPs was ca. 135 ± 15 nm (114 ± 10 nm by TEM, Figure 1c), with a spherical shape and a zeta potential of ca. $+15.2 \pm 0.9$ mV. The observed differences in size between DLS and TEM arise from the drying process and subsequent shrinkage polymeric chains underwent during TEM sample preparation. A negligible size variation was observed upon ICG complexation to give DXSP-PLGA-ICG hybrid NPs, which possessed a net zeta potential of -29.1 ± 2.5 mV pointing to the successful complexation of ICG molecules. This was additionally corroborated by the presence of a fluorescence emission peak at ca. 820 nm, typical of ICG molecules (Figure S4).

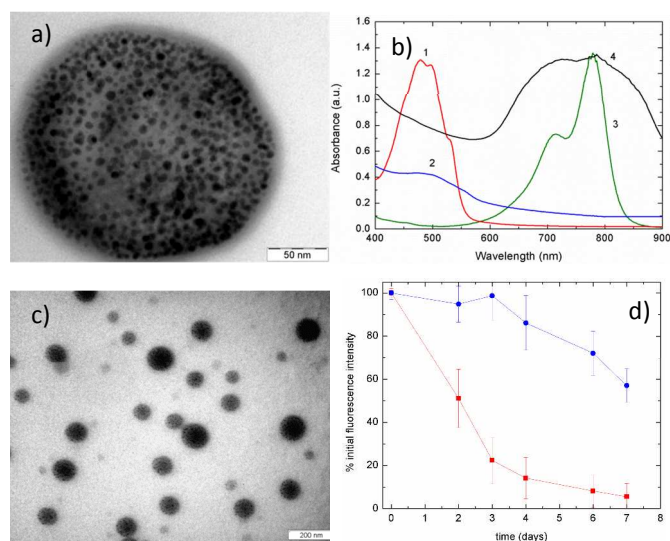


Figure 1. a) TEM image of a DXSP-PLGA NP. b) UV-Vis spectra of 1) free DOXO, 2) DXSP-PLGA NPs, 3) free ICG and 4) DXSP-PLGA-ICG NPs. c) TEM image of DXSP-PLGA-ICG NPs. d) Fluorescence stability of (■) free ICG and (●) ICG complexed to PLGA NPs. In d) lines are to guide the eye.

DXSP-PLGA-ICG NPs also remained stable upon extensive incubation under serum containing medium of physiological pH as observed from the negligible changes in NP size pointing to the capability of the F127 stealth layer to avoid protein binding and subsequent NP aggregation.²⁷ Conversely, under acidic

conditions the larger hydrolytic degradation rate of PLGA chains involved a slightly decrease in NP stability at the end of the incubation period (Figure S5). We observed the strong complexation of ICG to the nanoplatform surface protect the dye from degradation, as observed from the fluorescence intensity of complexed ICG after 7 days if compared to that of free ICG (Figure 1d).²⁸

Exposure of aqueous suspensions of DXSP-PLGA-ICG NPs to continuous NIR illumination at a laser power of 2.5 W cm^{-2} for 5 min resulted in an elevation of solution mean temperature able to produce cytotoxic cell hyperthermia. No important temperature changes were observed when bare PLGA NPs were exposed to NIR light (Figure 2a). Conversely, aqueous dispersions of DXSP-PLGA-ICG NPs containing 1, 4 and 8 μM of ICG achieved temperature elevations of 4 $^{\circ}\text{C}$, 8 $^{\circ}\text{C}$ and 14 $^{\circ}\text{C}$, respectively. Due to photo- and thermal degradation, there existed a slow temperature decline after 8 min of laser irradiation. Hence, at concentrations above 4 μM ICG hybrid NPs can be easily heated up above 45 $^{\circ}\text{C}$, which is sufficient to induce irreversible damage to tumor cells but not normal cells, probably as a consequence of protein denaturation and poor DNA synthesis and repair due to the comparatively lower oxygen level and pH in cancerous cells.²⁹ These results suggest these nanoplatforms could act as efficient NIR-light absorbers for photothermal tumor therapy. In addition, DXSP-PLGA-ICG NP dispersions achieved a more efficient laser-dependent temperature response than free ICG at similar concentrations due to a higher condensed concentration of ICG molecules on the NP surfaces than free ICG, which results in a higher energy efficiency and lower heat dissipation after laser irradiation.³⁰ The morphology of hybrid NPs after irradiation was, at least, partially conserved as observed by TEM images (Figure 2b). Drug molecules and some SPIONs were released probably as a result of partial melting of the polymeric core upon heating.

The present nanoplatforms also displayed robust magnetic properties as a consequence of SPION clustering inside the polymeric matrix.^{31,32} At 5 K, the thermal energy is not sufficient to induce magnetic moment randomization, thus, the nanoconstructs show typical ferromagnetic hysteresis loops with a remanence of 17.5 emu g^{-1} and a coercivity of $254 \pm 9 \text{ Oe}$ (Figure S6a). However, at 300 K the thermal energy is enough to randomize the magnetic moments leading to a decrease of the magnetization and to no remanence or coercivity, thereby, the hybrid NPs possess superparamagnetic behavior (Figure S6b). The saturation magnetization, μ_{sat} , of the nanoplatforms at 300 K was 60.7 emu g^{-1} , which is higher than values reported for other Au- Fe_3O_4 or Au- $\gamma\text{-Fe}_2\text{O}_3$ NPs.³¹⁻³⁴ Also, the μ_{sat} of the nanoplatforms was observed to be lower than that of classical singly dispersed SPIONs possibly as a consequence i) the diamagnetic mass of the polymer, and ii) the presence of canted or noncollinear surface spins.^{33,35}

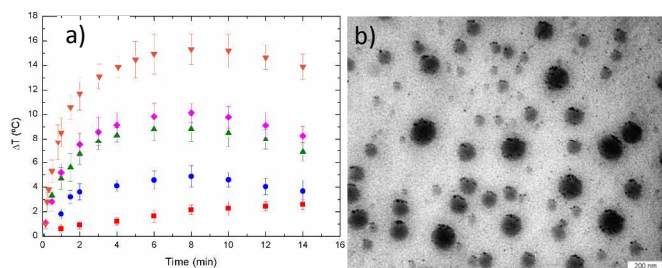


Figure 2. a) Temperature increments as a function of time under NIR light irradiation (2.5 W cm^{-2} , 5 min at 808 nm) for aqueous solutions of (■) bare PLGA NPs; (◆) 8 μM free ICG, and DXSP-PLGA-ICG NPs containing (●) 1, (▲) 4 (▼) and 8 μM conjugated-ICG. b) TEM image of DXSP-PLGA-ICG NPs after irradiation (2.5

W cm^{-2} , 5 min at 808 nm).

To evaluate the potential T_2 enhancing capability of these hybrid NPs, DXSP-PLGA-ICG with various iron concentrations were investigated by T_2 -weighted MR imaging at 9.4 T and 400 MHz. Figure S6c shows the T_2 -weighted MR images of the hybrid NPs in aqueous media at different Fe concentrations ranging from 0.01 to 0.17 mM. The signal intensity of the MR images decreased as the Fe concentration increased, as expected for T_2 contrast agents due to the shortening of spin-spin relaxation time of water, as commented previously. The specific relaxivity, r_2 , was determined to be 255 $\text{mM Fe}^{-1} \text{ s}^{-1}$ for DXSP-PLGA-ICG NPs. The relatively high r_2 value could be due to the large external magnetic field (9.4 T) applied to the nanoplatforms as well as their superior magnetic properties due to enhanced magnetic interactions between clustered SPIONs inside the polymeric matrix. It is worth noting that the obtained r_2 value was higher than that of commercially T_2 MRI contrast agents based on functionalized Fe_3O_4 NPs such as Feridex/Endorem ($r_2 = 160 \text{ mM Fe}^{-1} \text{ s}^{-1}$), Resovist ($r_2 = 151 \text{ mM Fe}^{-1} \text{ s}^{-1}$) and Sinerem ($r_2 = 160 \text{ mM Fe}^{-1} \text{ s}^{-1}$)^{36,37} and rather similar as those of other clustered-based magnetic nanoplatforms.^{15,16,34}

On the other hand, DOXO release kinetics could be fine-tuned by simply changing the molecular weight of the PLGA core (see Supporting Information and Figure S7a for further details). Hence, we decided to use PLGA NPs composed of a relatively large molecular weight PLGA polymer (38-54 kDa) to reduce drug leakage during the burst phase. *In vitro* cumulative DOXO release profiles at both neutral and acidic conditions in the presence of 10% (v/v) FBS showed a burst followed by a much slower diffusion-initiated release pattern (Figure 3). At pH 7.4, ca. 17% DOXO was released from NPs during the first 5 h of incubation and, then, a more sustained release was observed, with ca. 38% released at 48 h. The DOXO release could be enhanced upon irradiation of the hybrid NPs with NIR light (2.5 W cm^{-2} for 5 min), achieving 21 and 54% after 5 and 48 h of incubation, respectively; this result confirmed that drug release from the present hybrid NPs can be controllable by NIR-laser irradiation. This enhancement can be a consequence of the larger diffusion of the drug through the polymeric matrix upon temperature elevation (PLGA glass-transition temperature is ca. 45 $^{\circ}\text{C}$). Under acidic pH 5.5 DXSP-PLGA-ICG NPs released ca. 37% of the initially loaded DOXO during the first 5 h and ca. 58% after 48 h of incubation, respectively. The faster release under acidic conditions can be originated from the reprotonation of the amine group of DOXO, which involves an increase in its hydrophilicity and subsequent affinity decrease for hydrophobic polymeric chains, and an enhanced hydrolytic rate of PLGA chains under these conditions.³⁸ This, in turn, favors its escape from the NP core by an out-diffusion process through the core-shell structure whose diffusion rate depends on factors such as copolymer crystallinity, viscosity, and drug association state.³⁹ These larger release rates under acidic conditions would be beneficial to selectively release the drug from the DXSP-PLGA-ICG NPs in the acidic solid tumor microenvironment after passive cellular uptake.⁴⁰ The observed incomplete cumulative release of DOXO results from the combination of a relatively short duration of release studies and strong polymer-drug interactions, which make the NP matrix more rigid hindering the drug release.^{41,42}

On the other hand, in the time course of the release experiments a low amount of ICG was noted to be released at either of the tested conditions, which points to the strength of the electrostatic interactions between the sulfonate and amine groups of the dye and LMW-chitosan chains adsorbed on the NP surface, respectively (Figure S7b), as observed in related systems.⁴³ Meanwhile, a negligible release of SPIONs was observed under

similar solution conditions.

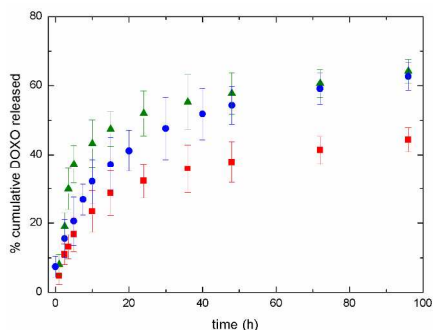


Figure 3. *In vitro* release kinetics of DOXO from DXSP-PLGA NPs (PLGA $M_w = 38$ -54 kDa) in aqueous serum-containing (10% FBS) medium of pH 7.4 in the absence (■) and presence (●) of irradiation (2.5 W cm^{-2} , 5 min at 808 nm), and of pH (▲) 5.5 in the absence of irradiation.

The uptake and cellular distribution of DXSP-PLGA-ICG NPs were analysed by confocal microscopy. After 2 h of cell incubation in the presence of DXSP-PLGA-ICG NPs gave rise to a granular fluorescence pattern in the cytoplasm in contrast to the observed continuous fluorescence pattern observed in cell nuclei upon administration of free DOXO.^{44,45} This observation might be originated, on one hand, from a relatively low amount of DOXO released from the hybrid NPs (see Figure 3) and, on the other, from a different internalization pathway of hybrid NPs if compared to free drug (Figure 4), probably through some type of endocytosis-mediated mechanism. DXSP-PLGA-ICG NPs might be initially located within endosome vesicles and would release DOXO in the cytosol in a sustained manner due to the endosome acidic environment; meanwhile size limitations would prevent hybrid NPs from traversing the nuclear pore complex, eventually impeding the drug to enter the cell immediately after administration. Nevertheless, some fluorescence can be already observed inside some cell nuclei corresponding to released DOXO to exert its antitumoral activity.

The uptake of the hybrid NPs could be also easily followed by the fluorescence emission of the complexed ICG dye in the nanoplateforms. The cell cytoplasm appears coloured due to the dye emission fluorescence signal (in this case selected green-coloured). It is worth mentioning that a complete colocalization of both DOXO and ICG fluorescence signals is not uniformly present around cell nuclei. It is necessary to bear in mind that DOXO fluorescence is largely enhanced when DOXO is released from the polymeric matrix as a consequence of self-quenching when inside.³¹ In addition, some ICG molecules could be also released to the cytoplasm from NPs and mainly bonded to intracellular proteins (glutathione S-transferase), as deduced from the expanded green fluorescence pattern in parts of the cell cytoplasm (Figure 4b).⁴⁴

On the other hand, when an external magnetic field is applied to the cell culture an enhancement of DOXO fluorescence was also observed. The increase in fluorescence would then stem from the increase in NPs accumulated inside the cells, which effectively deliver larger amounts of the chemotherapeutic drug and increase its local concentration (Figure S8a). This fact is additionally confirmed by T_2 -weighted MR images obtained using a 9.4 T clinical MRI system on HeLa cells treated with the hybrid NPs in the presence of an applied external magnetic field (Figure S8b).

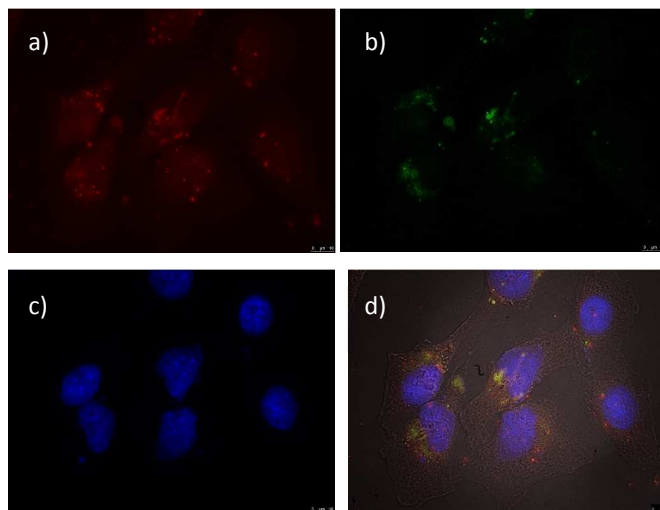


Figure 4. Fluorescence microscopy images of cellular uptake and intracellular distribution of DXSP-PLGA-ICG NPs. a) DOXO fluorescence (red-coloured, $\lambda_{exc} = 488 \text{ nm}$); b) ICG fluorescence (green-coloured, $\lambda_{exc} = 712 \text{ nm}$); c) Blue fluorescence from cell nuclei stained with DAPI ($\lambda_{exc} = 355 \text{ nm}$); d) merged images plus bright field channel. Scale bar is $20 \mu\text{m}$.

We further quantitatively evaluated the multidimensional therapeutic potential of the present hybrid NPs based on the combination of localized hyperthermia under ICG excitation by NIR laser irradiation and DOXO chemotherapy. Cervical HeLa and breast MDA-MB-231 cancer cells were incubated in the presence of free DOXO and SPION-PLGA-ICG (SP-PLGA-ICG) as controls and DXSP-PLGA-ICG NPs, and a crystal violet cell cytotoxicity assay was performed provided that DOXO can cause interferences with formazan crystals when using the standard MTT cell proliferation assay.⁴⁶

Cell viabilities (CV) of both types of cells treated with the bare NPs (SP-PLGA-ICG) at different NP concentrations after 24 h of incubation in the absence of NIR irradiation were almost negligible as observed in Figure 5a (orange bar) and Figure S9, confirming that these NPs can be considered as biocompatible. DXSP-PLGA-ICG NPs in the absence of irradiation possessed a slightly larger toxicity than SP-PLGA-ICG, which depend on NP concentration (Figure 5a, blue column), *i.e.* on the loaded DOXO concentration inside the polymeric matrix core and ICG content. Also, incubation of both cell lines with different concentrations of free DOXO resulted in slightly larger viabilities compared with DXSP-PLGA-ICG NPs containing the same amount of drug. This can result from the existence of opposite effects: On one hand, intracellular NP-released DOXO concentration could be enhanced by i) circumventing the multidrug resistance (MDR) effect which can appear when DOXO is administered as a free drug,⁴⁷ and ii) an enhanced internalization of the hybrid NPs into cells through inespecific endocytosis, if compared to a passive diffusion mechanism of the free drug,⁴⁸ conversely, the DOXO concentration inside cells can be reduced by the sustained drug release from the NPs, which is more important at short incubation times.

When exposing the cells to NIR laser illumination (2.5 W cm^{-2} for 5 min at 808 nm) in the presence of DXSP-PLGA-ICG NPs CVs decreased up to 93% at the highest measured NP concentration ($12.5 \mu\text{M}$ DOXO) compared with those cells bearing DXSP-PLGA or SP-PLGA-ICG NPs under similar illumination conditions (ca. 20 and 40% at 24 h, respectively). These larger cell mortalities appeared when the solution temperature raised above $43 \text{ }^\circ\text{C}$ upon irradiation,

at which tumor cells are damaged probably by denaturation of intracellular proteins.⁴⁹ Notably, DXSP-PLGA-ICG NPs exhibited an additional cytotoxic effect ($(CV_{SP-PLGA-ICG+NIR} - CV_{DXSP-PLGA-ICG+NIR})/CV_{SP-PLGA-ICG+NIR}$) of up to 91% (at 12.5 μ M DOXO) when compared to SP-PLGA-ICG NPs due to the remote release of DOXO, which was more important as the amount of DOXO increased in solution. Therefore, it seems that the simultaneous combination of NIR hyperthermia provided by ICG excitation and the chemotherapeutic action of DOXO can result in an enhanced cytotoxic effect. Apart from the inherent hyperthermia cytotoxicity (as denoted when compared irradiated to non-irradiated SP-PLGA-ICG NPs), the observed larger cytotoxicity might be also caused by an altered kinetics, permeability and uptake of the chemotherapeutic agent during the heating process.⁵⁰ In this regard, the photothermal effect of ICG might help to partially melt the core of the PLGA polymeric matrix, releasing a larger amount of DOXO from DXSP-PLGA-ICG NPs (as observed in drug release experiments, see Figure 3). The cytotoxicity of DXSP-PLGA-ICG NPs was observed to be additionally enhanced (from 67 to 77% after 24 h of incubation in the presence of 2.5 μ M DOXO, see for example Figure 5b) when an external magnetic field was applied to cells, probably allowing NP attraction near cells and, thereby, increasing the NPs internalization and the localized DOXO release and photothermal effect inside cells, as previously mentioned.^{51,52}

After 24 h of additional incubation with the different typers of NPs (48 h in total, 2.5 μ M DOXO and 4.0 μ M ICG, respectively) CVs were also examined revealing additional systemic cytotoxicity. Cell viabilities of cells treated with DXSP-PLGA-ICG NPs was additionally decreased due to the combined inhibitory effects of targeted hyperthermia, sustained DOXO release and magnetic guiding (Figure 5b and Figure S9b). In this case, the CV was 22% decreasing up to 7% when the external magnetic field was applied to MDA-MB-231 cells, with a targeting tumoricidal effect of ca. 32% ($(CV_{DXSP-PLGA-ICG+NIR} - CV_{DXSP-PLGA-ICG+NIR+magnetic\ field})/CV_{SP-PLGA-ICG+NIR}$). Similar trends were also observed for HeLa cells (see Figure S9) indicating the good cytotoxic performance of the present nanoplatforms independently of the cancerous cell type used in the present *in vitro* studies.

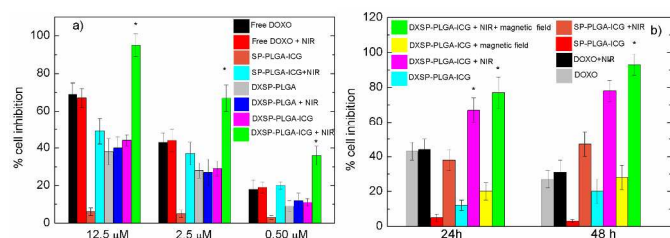


Figure 5. a) MDA-MB-231 cell inhibition of free DOXO, SP-PLGA-ICG NPs, DXSP-PLGA NPs, DXSP-PLGA-ICG NPs, DXSP-PLGA-ICG NPs in the absence and presence of continuous NIR light (808 nm) of 2.5 W cm^{-2} for 5 min at different NP concentrations (expressed in DOXO content). b) MDA-MB-231 cell inhibition of free DOXO, SP-PLGA-ICG NPs, DXSP-PLGA-ICG NPs, DXSP-PLGA-ICG NPs in the absence and presence of continuous NIR light (808 nm) of 2.5 W cm^{-2} for 5 min after 24 h and 48 h of incubation at a DOXO content in NPs of 2.5 μ M. Yellow and green column also indicates cell inhibition of DXSP-PLGA-ICG NPs in the presence of an external applied magnetic field. Data shown as mean \pm SD (n=3).

As a preliminary step, we here performed a qualitative preliminary analysis of the *in vivo* biodistribution and potential use

as an imaging fluorescent probe of the present nanoplatforms after a single intravenous injection (at the tail vein) in a tumor-bearing MDA-MB-231 BALB/c nude mice model. When the tumor reached approximately 100 mm^3 in size, intravenous administration of 10 mg/kg of SP-PLGA-ICG NPs into the mouse tail vein was performed. Accumulation of SP-PLGA-ICG NPs in the tumor region took place in a very short time interval (2 h) probably through the EPR effect. A relatively higher fluorescence signal could be observed in the RES area, mainly in liver and spleen, and lung (Figure 6 and Figure S10). In contrast, a much lower fluorescence from free ICG administered as a control is observed due to its known blood instability and extremely short *in vivo* half-life (ca. 150-180 s).⁵³ In fact, only traces of free ICG fluorescence were already detected after 48 h post-injection (image not shown). Also, SP-PLGA-ICG NPs suitably stabilized ICG molecules avoiding their rapid photo-degradation and aqueous instability *in vivo*; if this would occur low molecular weight components would be filtered from the blood by the kidneys, which can then would be rapidly and massively detected in the bladder region; therefore, early detection of very large fluorescence signals in the bladder region at short times post-injection be a indication of dye detachment from the platform and, subsequently, of their instability *in vivo*.⁵⁴

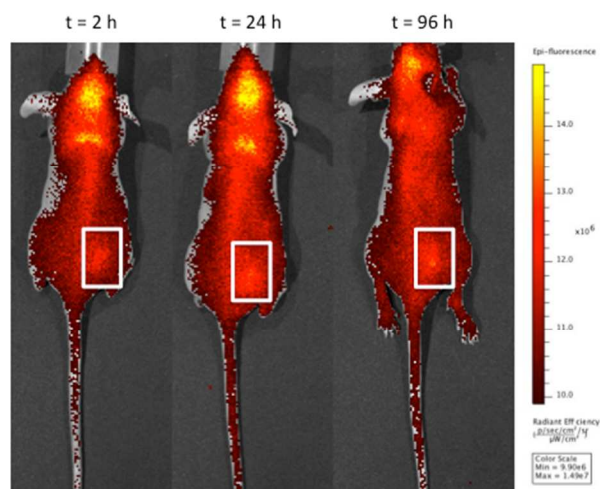


Figure 6. Time-lapse *in vivo* NIR images of MDA-MB-231 breast adenocarcinoma tumor-bearing mouse after intravenous tail injection of DXSP-PLGA-ICG NPs. The squared region denotes the tumor localization.

Also, the present observations indicate the need of developing an additional targeting strategy to enhance nanoplatform accumulation in the tumor region and decrease its diffusion along the rest of the body when analysing the *in vivo* performance of the present particles as theranostic nanoplatforms, which will be subject of a forthcoming publication. The choice of targeting ligands which would bind with larger affinity to overexpressed receptors in MDA-MB-231 cells such as epidermal growth factor receptor, CD44, $\alpha_v\beta_3$ integrin or transforming growth factor alpha (TGF- α) might be an option to enhance targeting efficiency.⁵⁵⁻⁵⁶ On the other hand, it is worth mentioning the existence of fluorescence around the mice's head which suggests nanoplatforms might be also accumulated in the brain area (Figure 6). In this regard, some previous studies have shown that surface NP coating is a key factor to overcome the blood brain barrier (BBB) and achieve successful brain delivery.⁵⁷ Pluronic-F68 or polysorbate-coated PLGA NPs have been shown to effectively delivery DOXO to intracranial glioblastoma in rats⁵⁸

through the enhanced adsorption of apolipoprotein A-I on the NP surface which interacts with the scavenger receptor SR-BI at the BBB endothelium, facilitating BBB crossing. Therefore, the presence of Pluronic F127 on the chitosan stabilizing adlayer of our hybrid NPs might play a role to allow brain accumulation. By contrast, HSA or PVA-stabilized PLGA NPs were found to exert a negligible effect on tumor suppression.⁵⁹ However, additional tests and more detailed tests are required to confirm this hypothesis and will be the subject of a forthcoming publication.

At longer times after i.v. injection of nanoplateforms, a relatively important proportion of the initial fluorescence around the tumor area was still retained, even after 96 h post-injection (Figure 6). Some fluorescence in the bladder region is still retained indicating that some little fragments from the biodegraded NPs might be also excreted via renal clearance after polymer degradation in plasma and subsequent ICG released. The fluorescent signal from RES organs and brain progressively decreases (see Figure S10), which is compatible with nanoparticle degradation and clearance mainly through hepatobiliary excretion route, as denoted by 3-D image reconstruction of RES organs, where NPs are observed to be accumulated mainly in the spleen and, to lesser extent, in the liver (Figure S11), with no traces in lungs at 96 h post-injection. This was further confirmed by ultrastructural TEM images of sectioned slices of liver, spleen, lung, kidney and tumor post-injection from which no signs of nanoparticle accumulation were observed (Figure S12); only the presence of some released SPIONS probably from the degradation of the PLGA matrix are observed. In addition, the histopathological analysis performed using hematoxylin and eosin (H&E) staining shows no pathological lesions or structural modifications. Moreover, the immunostaining of activated-caspase 3, as an apoptosis marker, demonstrate the absence of apoptosis in liver and tumor tissues after 96h post-injection, which additionally denote the absence of cellular apoptosis and the subsequent cytocompatibility of the present nanoplateforms (Figure S13), respectively.

C Experimental Section

C1 Materials.

Poly(D,L-lactide-co-glycolide) (PLGA) of different molecular weights (7-17 kDa; 24-38 kDa; 38-54 kDa and 40-75 kDa with 50:50 lactide-glycolide ratio; 4-14 kDa and 66-107 kDa with 75:25 lactide-glycolide ratio), poly-vinyl alcohol (PVA), Pluronic F127, hydrogen tetrachloroaurate (III) trihydrate (HAuCl₄), FeCl₂, FeCl₃ and ICG were purchased from Sigma-Aldrich (St. Louis, MO, USA). Low molecular weight chitosan (LMW-chitosan, M_w = 111 kDa) was purchased from Fluka (St. Louis, MO, USA). Oleic acid with 90% purity was purchased from Alfa Aesar (Karlshue, Germany). DOXO HCl and fetal bovine serum (FBS) were purchased from Fisher Scientific (Pittsburgh, PA, USA). ProLong® Gold antifade reagent with DAPI, Dulbecco's modified eagle medium, fetal bovine serum (FBS), L-glutamine, penicillin/streptomycin, sodium pyruvate, and MEM non-essential amino acids were purchased from Invitrogen (Carlsbad, USA). Dialysis membrane tubing (molecular weight cutoff ~3500) was purchased from Spectrum Laboratories, Inc. (Rancho Dominguez, CA, USA). All other chemicals and solvents were of reagent grade (from Sigma-Aldrich). Milli-Q grade water was used in all preparations.

C2 Synthesis of SPIONS

Oleic acid-stabilized SPIONS were synthesized by a

coprecipitation method. Briefly, aqueous solutions of 0.1 M FeCl₃ (30 mL) and FeCl₂ (15 mL) prepared with N₂ purged-water were mixed; then, 3 mL of 5 M ammonia solution were added in small aliquots of 0.6 mL while stirring. A black precipitate was formed indicating the formation of SPIONS. After 20 min of stirring under N₂ atmosphere, 56.4 mg of oleic acid were added to the SPIONS and the temperature was raised to 80 °C and kept for 30 min while stirring to evaporate the ammonia. The magnetic NPs were washed twice by centrifugation at 9000 rpm for 20 minutes to eliminate excess of oleic acid, the supernatant was discarded and the precipitate was lyophilized and stored at 4 °C.⁶⁰

C3 Synthesis of DXSP-PLGA-ICG NPs

In a typical preparation, PLGA (25 mg) was dissolved in a sealed vial containing acetone (4 mL) together with suitable amounts of DOXO (previously converted to its hydrophobic base form by addition of triethylamine as reported in literature)⁶¹ and SPIONS dispersed in acetone by sonication with a probe type sonicator (20 kHz, Bandelin Sonopuls, Bandelin GmbH, Berlin, Germany) at 20 W for 10 min in an ice bath. Then, this organic solution was added dropwise with a syringe pump (0.166 mL/min) to an aqueous solution (50 mL) containing Pluronic F127 (typically 1 wt. % if not otherwise stated) while stirring at 10 °C. After sonication at 100 W for 10 min in an ice bath to homogenize the resulting dispersion, the organic solvent was completely evaporated under mechanical stirring overnight, the dispersion subsequently centrifuged twice at 9000 rpm for 30 min and 20 °C. Subsequently, the supernatant was removed and the final precipitate was resuspended in 5 mL of water. ICG was complexed to the DXSP-PLGA NPs by electrostatic interactions with positively charged low molecular weight chitosan (LMW-chitosan) displayed on the surface of the DXSP-PLGA NPs. First, 5 mL of DXSP-PLGA NPs suspension were mixed with 0.25 mL of 1 wt. % LMW-chitosan previously dissolved in 1% (v/v) acetic acid. After stirring for 4 h, DXSP-PLGA NPs were centrifuged twice at 9000 rpm for 30 min to eliminate free and loosely adsorbed chitosan. Then, the DXSP-PLGA NPs were mixed with 5 mg of ICG previously dissolved in 5 mL water and stirred 4 h at ambient temperature. Then, the sample was washed by centrifugation three times at 9000 rpm for 30 min at 20 °C to eliminate excess of ICG, whose concentration in the supernatant was spectrophotometrically measured in order to have an initial estimation of the amount of complexed dye. Subsequently, the supernatant was discharged and the pellet of DXSP-PLGA NPs with electrostatically bound ICG (DXSP-PLGA-ICG NPs) was redispersed in 5 mL of water, lyophilized and stored at 4 °C.

C4 Characterization of NPs

NP sizes were obtained by dynamic light scattering (DLS) at 25 °C by means of an ALV-5000F (ALV-GmbH, Germany) instrument with vertically polarized incident light ($\lambda = 488$ nm) supplied by a diode-pumped Nd:YAG solid-state laser (Coherent Inc., CA, USA) operated at 2 W, and combined with an ALV SP-86 digital correlator (sampling time 25 ns to 100 ms). Experiment duration was in the range 5-10 min, and each experiment was repeated at least three times. Sizes and morphologies of the NPs were also acquired by transmission and scanning electron microscopy (TEM and SEM, respectively) by means of a Phillips CM-12 and a Carl Zeiss Libra 200 Fm Omega (TEM), and a FESEM Ultra Plus electronic microscopes operating at 120 and 20 kV,

respectively. NPs zeta potential was measured by triplicate with a Zetasizer Nano ZS (Malvern, UK), using disposable folded capillary cells. UV-Vis and fluorescence spectroscopy spectra of the particles were performed in a Cary 100 Bio and Cary Eclipse spectrophotometers (Agilent Technologies, Santa Clara, CA, USA), respectively. X-ray diffraction (XRD) experiments were carried out with a rotating anode X-ray generator (Siemens D5005, Germany). Twin Göbel mirrors were used to produce a well-collimated beam of CuK α radiation ($\lambda = 1.5418 \text{ \AA}$). X-ray diffraction patterns were recorded with an imaging plate detector (AXS F.Nr. J2–394). The concentration of PLGA NPs was determined from the solvent's and the sample's specific viscosities (see Electronic Supplementary Information for details).

C5 Cargo Entrapment efficiency and loading capacity

To exactly quantify the extent of DOXO loading and ICG conjugation, DXSP-PLGA-ICG NPs were weighted and dissolved in dimethylsulfoxide (DMSO). ICG and DOXO fluorescence calibration curves were prepared prior to measurements to verify spectral characteristics, linearity range, and possible overlap between the spectra of the two compounds. Samples were placed in quartz-0.5 mL cuvettes, and measurements were performed immediately after preparation. DMSO was used as a blank for background correction. The excitation wavelengths were 760 nm for ICG and 490 nm for DOXO, respectively, and spectral emission readings were recorded in 1-nm intervals from 510 nm to 700 nm for DOXO and from 790 to 900 nm for ICG. All measurements and sample handling were done in reduced lighting conditions, and the instrument operating conditions were kept constant. The concentrations of ICG and DOXO were determined from the corresponding blank-subtracted reading at the peak emission wavelength, by using the previously obtained calibration curves of ICG and DOXO in DMSO. Drug loaded/conjugated, D.L., and entrapment efficiency, E.E., in the DXSP-PLGA-ICG NPs were calculated as follows:

$$D.L. \% = \frac{\text{weight of DOXO, SPIONs or ICG in NPs}}{\text{weight of NPs}} \times 100 \quad (1)$$

$$E.E. \% = \frac{\text{weight of DOXO, SPIONs or ICG in NPs}}{\text{weight of DOXO, SPIONs or ICG initially loaded}} \times 100 \quad (2)$$

To quantify SPIONs loading capacity and entrapment efficiency DXSP-PLGA NPs were dissolved in 500 μL of concentrated HNO_3 (68%) and the solution volume was raised to 5 mL with a 20% HNO_3 solution for total Fe quantification.

C6 In vitro release kinetics

Aliquots (5 mL) of 0.4 wt.% DXSP-PLGA and PLGA/ICG NPs in phosphate-buffered saline (PBS) pH 7.4, or sodium citrate-citric acid buffer pH 5.5, and complemented with 10% (v/v) of FBS were placed in a temperature controlled bath at 37 $^\circ\text{C}$ and stirring speed of 100 rpm. The total amount of both DOXO and ICG in the NPs was kept below 10% of the cargo solubility limit in PBS in order to ensure sink conditions.⁶¹ The tubes were collected at regular time intervals and centrifuged at 9000 rpm for 20 min, followed by lyophilization of the pellet for 36 h. Remaining cargo (ICG or DOXO) in the polymeric NPs was measured by dissolving the NP pellet in DMSO for 24 h. The percentage of ICG and DOXO released at a certain time interval was calculated by the following

equation:

$$\% \text{ ICG or DOXO released} = 100 - (\% \text{ ICG or DOX remaining}) \quad (3)$$

C7 Laser irradiation experiments

Temperature increment tests were performed with a continuous wave fiber-coupled diode laser source of 808 nm wavelength (50W, Oclaro Inc, San Jose, CA, USA). The laser was powered by a Newport 5700-80 regulated laser diode driver (Newport Corporation, Irvine, CA, USA). A 5 m-long, 200- μm -core optical fiber was used to transfer laser power from the laser unit to the target solution, and equipped with a lens telescope mounting accessory at the output, which allowed the tuning of the laser spot size in the range 1-10 mm. The output power was independently calibrated using an optical power meter (Newport 1916-C), and the laser spot size was previously measured with a laser beam profiler (Newport LBP-1-USB) placed at the sample's plane. For measuring the temperature change mediated by the present hybrid NPs, 2 mL of hybrid DXSP-PLGA-ICG NPs were placed in a quartz cuvette and irradiated for determined time intervals and/or at different power intensities. The sample temperature was measured with a type J thermocouple linked to a digital thermometer inserted into the solution. Bare PLGA NPs in water were used as a control.

C8 Magnetic resonance imaging and magnetic susceptibility

An 1.6% (w/v) agarose solution was heated and stirred at 80 $^\circ\text{C}$ until complete dissolution of the solid agarose. Then, while the system was fluid, an array of seven centrifuge tubes (1.5 mL) were placed within the agarose, which was slowly cool down to room temperature. After solidification, the tubes were removed and an agarose mold with seven holes was obtained. For cell imaging, HeLa cells ($2 \cdot 10^6$ cells) were seeded in 75 cm^2 flasks and cultured for 24 h at standard conditions (5% CO_2 at 37 $^\circ\text{C}$) in Dulbecco's Modified Eagle Medium (DMEM) supplemented with 10% (v/v) FBS, 2 mM L-glutamine, 1% penicillin/streptomycin, 1 mM sodium pyruvate, and 0.1 mM MEM Non-Essential Amino Acids (NEAA). Then, the medium was replaced with fresh one containing DXSP-PLGA-ICG NPs and incubated for 6 h; then, the medium with NPs was removed and cells were washed with PBS and incubated for additional 18 h. Afterwards, cells were trypsinized and resuspended in 100 μL of PBS. In each hole of the phantom a mixture of cells labeled with DXSP-PLGA-ICG NPs and 2% (w/v) agarose was set. After a resting period, 1.6% (w/v) agarose was added to the mold to seal the phantom holes. Imaging of the phantoms was performed acquiring a 3D-gradient echo image (T_2 -weighting) with the following parameters: field of view, 80 \times 80 \times 40 mm; matrix size: 512 \times 512 \times 256 points giving a spatial resolution of 156 \times 156 \times 156 μm ; echo time TE = 7.89 ms and repetition time TR = 100 ms; flip angle 20 degree and 2 averages. On the other hand, magnetic susceptibility measurements were carried out with a SQUID magnetometer (Quantum Design MPMS5, San Diego, CA, USA) at 5 and 300 K.

C9 Cellular uptake

DXSP-PLGA-ICG NPs cellular uptake was followed by confocal microscopy by seeding HeLa cells (Cell Biolabs, San Diego, CA, USA) on poly-L-lysine coated glass coverslips (12 \times 12 mm) placed inside 6-well plates (3 mL, $5 \cdot 10^4$ cells per well) and grown for 24 h at standard culture conditions. Then, DXSP-PLGA-

ICG NPs (200 μL , $\sim 5.0 \cdot 10^8$ particles mL^{-1}) were added to cells. In some wells, a magnet of 0.5 T was placed below each individual well to analyse the effect of an applied magnetic field on cellular internalization. After 2 h of incubation with DXSP-PLGA-ICG NPs, cells were washed with PBS, fixed with paraformaldehyde 4% (w/v) for 10 min, washed and stained with BODIPY Phalloidin (Invitrogen) in 0.2% (w/v) Triton X-100 (permeabilizer). The cells were washed again with PBS pH 7.4, mounted on glass slides and stained with ProLong Gold antifade DAPI (Invitrogen) and cured for 24 h at -20°C . Samples were visualized at 63X using a confocal spectral microscope Leica TCS-SP2 (LEICA Microsystems Heidelberg GmbH, Mannheim, Germany; green channel for DOXO, λ_{exc} 488 nm, and red channel for BODIPY Phalloidin, λ_{exc} 633 nm); blue channel for DAPI, λ_{exc} 355 nm. A similar protocol was also performed to observe the internalization of the NPs following the fluorescence of ICG (λ_{exc} = 785 nm) without BODIPY Phalloidin to avoid overlapping of emissions.

C10 *In vitro* cytotoxicity

HeLa cells with an optical confluence of 80–90% were seeded into 96-well plates (100 μL , 1.5×10^4 cells per well) and grown for 24 h at standard culture conditions (5% CO_2 at 37°C) in Dulbecco's Modified Eagle Medium (DMEM) supplemented with 10% (v/v) FBS, 2 mM L-glutamine, 1% penicillin/streptomycin, 1 mM sodium pyruvate, and 0.1 mM MEM Non-Essential Amino Acids (NEAA). Afterwards, DXSP-PLGA-ICG NPs and corresponding controls (free DOXO, DOXO-loaded PLGA NPs and SP-PLGA-ICG NPs) were injected in the wells (100 μL) and incubated for 24 h and 48 h in the presence and absence of an applied external field provided by a magnet (= 0.5 T) placed at the bottom of the wells. After incubation, the culture medium was discarded and the cells were washed with 10 mM PBS, pH 7.4, several times. The cells were shaken at room temperature (300 rpm, 15 min) in the presence of 10 μL of a glutaraldehyde solution (11% (w/v) in water). The solution was discarded and cells were washed 3–4 times with milli-Q water. The cells were then shaken at room temperature (300 rpm, 15 min) in the presence of 100 μL of a crystal violet solution (0.1% (w/v) in 200 mM orthophosphoric acid, 200 mM formic acid, and 200 mM 2-N-morpholino-ethanesulfonic acid (MES), pH 6). The solution was discarded, and the cells were again washed 3–4 times with milli-Q water. Once washed, the cells were left for incubation at room temperature overnight for drying. Once dried, the cells were shaken at room temperature (300 rpm, 15 min) in the presence of 100 μL of acetic acid (10% (v/v) in water). Immediately after, the absorbance of the resulting solution was measured with a Microplate Reader (FLUOstar Optima, BMG Labtech GmbH, Germany) operating at 595 nm. All experiments were triplicate carried out. The growth inhibition was quantified as:

$$\% \text{ Inhibition} = 100 - \frac{100 \cdot \text{OA}}{\text{TA}} \quad (4)$$

where OA and TA stand for the absorbance of studied samples and negative controls (cells in the absence of NPs), respectively.

C11 *In vivo* near-infrared fluorescence imaging

Mice were housed in specific pathogen-free (SPF) conditions, following FELASA (Federation of European Laboratory Animal Science Associations) guidelines for animal housing. The care and use of all experimental animals was in accordance with institutional guidelines and approved by the Ethics Committee of the University of Santiago de Compostela and Xunta de Galicia (approval ID

15005AE/07/FUN01/FIS02/JACP1).

To assess the *in vivo* performance of the nanoparticles $3 \cdot 10^6$ cells from MDA-MB-231 adenocarcinoma breast cell line⁶² were injected in the dorsal flank of immunodeficient BALB/c nude mice. One week upon injection, cell implantation was checked by registering the fluorescent and bioluminescent activity of the cells. Prior to treatment with the nanoplateforms, mice were sedated with 150 mg/kg of 2,2,2-tribromoethanol (Sigma-Aldrich, USA). We next injected 10 mg kg^{-1} of either DXSP-PLGA-ICG NPs or free ICG in the tail vein and registered the *in vivo* fluorescent activity (λ_{exc} = 710 nm, λ_{em} = 840 nm) with a IVIS Spectrum imaging system (Caliper LifeSciences, Perkin-Elmer, USA) at 2, 4, 6, 24, 48 and 96 h upon NPs administration. Mice were anesthetized using isoflurane during image acquisition. D-Luciferin (Intrace Medical, Switzerland) was also administered (150 mg/kg) in order to co-localize the bioluminescence in tumour cells with the fluorescent from ICG.

C12 Histology and transmission electron microscopy (TEM)

Liver and tumour samples were collected ninety six hours post-injection. Samples were fixed in 10% formalin overnight and subsequently dehydrated in 70% ethanol and embedded in paraffin wax. Histological analysis included hematoxylin & eosin staining and cleaved caspase-3 immunostaining (#9661, Cell Signaling, USA). Samples for TEM were fixed in 2% glutaraldehyde (electron microscopy grade; Sigma-Aldrich, USA) in 0.2M HEPES pH 7.4 overnight, washed again in cacodylate buffer 0.1M pH 7.4, and postfixed with 2% osmium tetroxide in cacodylate buffer at RT for 1h. Organs were then embedded in agar, dehydrated with ethanol and finally embedded in EPON resin. Staining with uranyl acetate was purportedly omitted to avoid possible false positives.

Conclusions

The present results reveal that the combination of chemotherapy, magnetic targeting, and photothermal therapy through polymeric hybrid NPs is expected to significantly increase the likelihood and selectivity of cell killing. PLGA hybrid NPs might be guided to the tumor area by an applied magnetic field as observed *in vitro*, and the subsequent combination of NIR laser irradiation and chemotherapy at the tumor site would enhance their therapeutic effectiveness. One of the major advantages of NIR laser light as a source for localized hyperthermia is that light exposure is non-invasive and can be applied extracorporeally compared with other types of hyperthermia like radiofrequency or microwave ablation. The permeability of tumor vessels and the sensitivity of tumor cells toward chemotherapeutics should be greatly enhanced by hyperthermia, holding the promise of improving drug efficacy. Photothermal ICG-mediated therapy might facilitate triggered and instant drug release from the hybrid NPs, which is critical for achieving a high effective drug concentration in the tumor site. The luminescent properties of the present hybrid NPs also enabled to follow the particle localization and biodistribution *in vivo*, which corroborated the power of fluorescence NIR imaging as an excellent diagnostic and therapy monitoring tool.

Acknowledgements

Authors thank Ministerio de Economía y Competitividad (MINECO) for research project MAT 2010-17336, Xunta de Galicia for research grant CN2012/072, and Fundación Ramón Areces for additional financial support. Authors also specially thank staff of Instituto de Ortopedia y Banco de Tejidos Musculoesqueléticos, of the

Universidad de Santiago de Compostela, and specially to Maite Silva, for hepful assistance during *in vitro* cell experiments. S. B. greatly acknowledges MINECO for her Ramon y Cajal fellowship. A.T. and M.A.-M. thank Mexico's National Council of Science and Technology (CONACYT) for grants No.203907 and No. 203732, respectively.

Notes and references

^a Grupo de Física de Coloides y Polímeros, Departamento de Física de la Materia Condensada, Universidad de Santiago de Compostela, Santiago de Compostela, 15782, Spain.

^b Grupo de Oncología Molecular, Centro de Investigación en Medicina Molecular y Enfermedades Crónicas (CIMUS), Universidad de Santiago de Compostela, Santiago de Compostela, 15782, Spain.

^c Laboratorio de Investigación en Neurociencias Clínicas, Hospital Clínico Universitario de Santiago de Compostela, 15782, Spain.

*Authors to whom correspondence should be addressed: silvia.barbosa@usc.es; pablo.taboada@usc.es

†Present address: Catalanian Institute of Chemical Research, Avda. Països Catalans 16, Tarragona, 43007, Spain.

+3B's Research Group-Biomaterials, Biodegradables and Biomimetics, University of Minho, Headquarters of the European Institute of Excellence on Tissue Engineering and Regenerative Medicine, AvePark, Zona Industrial da Gandra, S. Claudio do Barco, Caldas das Taipas, Guimarães, 48-909, Portugal.

Electronic Supplementary Information (ESI) available: Quantification of polymeric NPs, effect of different parameters on the properties of polymeric NPs, characterization of SPIONs, fluorescence spectra, size evolution and release kinetics of hybrid NPs, fluorescence and MR imaging of NP cell internalization, 3D-reconstructed images of NP accumulation in mice tissues. See DOI: 10.1039/b000000x/.

- O. C. Farokhzad, R. Langer, *Adv. Drug Delivery Rev.* 2006, **58**, 1456.
- P. Y. Lee, K. Y. K. Wong, *Current Drug Deliv* 2011, **8**, 245.
- J. Heidel, M. Davis, *Pharm. Res.* 2011, **28**, 187.
- M. Shen, Y. Huang, L. Han, J. Qin, X. Fang, J. Wang, V. C. Yang, *J. Control. Release* 2012, **161**, 884.
- D. B. Shenoy, M. M. Amiji, *Int. J. Pharm.* 2005, **293**, 261.
- Q. Wu, S. Deng, L. Li, L. Sun, X. Yang, X. Liu, L. Liu, Z. qian, Y. Wei, C. Gong, *Nanoscale* 2013, **5**, 12480.
- J.-M. Lü, X. Wang, C. Marin-Muller, H. Wang, P. H. Lin, Q. Yao, C. Chen, *Expert Rev. Mol. Diagn.* 2009, **9**, 325.
- I. Armentano, M. Dottori, E. Fortunati, S. Mattioli, J. M. Kenny, *Polym. Degrad. Stab.* 2010, **95**, 2126.
- F. Danhier, E. Ansorena, J. M. Silva, R. Coco, A. Le Breton, V. Préat, *J. Control. Release* 2012, **161**, 505.

- R. C. Mundargi, V. R. Babu, V. Rangaswamy, P. Patel, T. M. Aminabhavi, *J. Control. Release* 2008, **125**, 193.
- I. Bala, S. Hariharan, M. N. Kumar, *Crit. Rev. Ther. Carrier Syst.* 2004, **21**, 387.
- R. A. Jain, *Biomaterials* 2000, **21**, 2475.
- A. S. Lübbe, C. Bergemann, W. Huhnt, T. Fricke, H. Riess, J. W. Brock, D. Huhn, *Cancer Res.* 1996, **56**, 4694.
- A. S. Lübbe, C. Bergemann, H. Riess, F. Schriever, P. Reichardt, K. Possinger, M. Matthias, B. Dörken, F. Herrmann, R. Gürtler, P. Hohenberger, N. Haas, R. Sohr, B. Sander, A.-J. Lemke, D. Ohlendorf, W. Huhnt, D. Huhn, *Cancer Res.* 1996, **56**, 4686.
- J. Yang, C.-H. Lee, J. Park, S. Seo, E.-K. Lim, Y. J. Song, J.-S. Suh, H.-G. Yoon, Y.-M. Huh, S. Haam, *J. Mater. Chem.* 2007, **17**, 2695.
- J. Kim, J. E. Lee, S. H. Lee, J. H. Yu, J. H. Lee, T. G. Park, T. Hyeon, *Adv. Mater.* 2008, **20**, 478.
- A. Singh, F. Dilnawaz, S. Mewar, U. Sharma, N. R. Jagannathan, S. K. Sahoo, *ACS Applied Materials & Interfaces* 2011, **3**, 842.
- N. Schleich, P. Sibret, P. Danhier, B. Ucakar, S. Laurent, R. N. Muller, C. Jérôme, B. Gallez, V. Préat, F. Danhier, *Int. J. Pharm.* 2013, **447**, 94.
- Y. qiu, R. Palankar, M. echeverría, N. Medvedev, S. E. moya, M. Delcea, *Nanoscale* 2013, **5**, 12624.
- S.-M. Lee, H. Park, J.-W. Choi, Y. N. Park, C.-O. Yun, K.-H. Yoo, *Angew. Chem. Int. Ed.* 2011, **50**, 7581.
- S.-M. Lee, H. Park, K.-H. Yoo, *Adv. Mater.* 2010, **22**, 4049.
- Y. Watanabe, K. Kumon, *J. Cardiothor. Vasc. Anesth.* 1999, **13**, 299.
- T. Desmettre, J. M. Devoisselle, S. Mordon, *Surv. Ophthalmol.* 2000, **45**, 15.
- S.-S. Feng, *Nanomedicine* 2006, **1**, 297.
- S. Acharya, S. K. Sahoo, *Adv. Drug Deliv. Rev.* 2011, **63**, 170.
- R. Savić, L. Luo, A. Eisenberg, D. Maysinger, *Science* 2003, **300**, 615.
- M. L. T. Zweers, G. H. M. Engbers, D. W. Grijpma, J. Feijen, *J. Control. Release* 2004, **100**, 347.
- A.-K. Kirchherr, A. Briel, K. Mäder, *Mol. Pharm.* 2009, **6**, 480.
- M. Paiva, D. J. Castro, M. Bublik, J. Sercarz, *J. Investig. Med.* 2006, **54**, S381.
- M. Zheng, C. Yue, Y. Ma, P. Gong, P. Zhao, C. Zheng, Z. Sheng, P. Zhang, Z. Wang, L. Cai, *ACS Nano* 2013, **7**, 2056.
- J. Kim, S. Park, J. E. Lee, S. M. Jin, J. H. Lee, I. S. Lee, I. Yang, J.-S. Kim, S. K. Kim, M.-H. Cho, T. Hyeon, *Angew. Chem. Int. Ed.* 2006, **45**, 7754.
- A. Gole, J. W. Stone, W. R. Gemmill, H.-C. zur Loye, C. J. Murphy, *Langmuir* 2008, **24**, 6232.
- E. V. Shevchenko, M. I. Bodnarchuk, M. V. Kovalenko, D. V. Talapin, R. K. Smith, S. Aloni, W. Heiss, A. P. Alivisatos, *Adv. Mater.* 2008, **20**, 4323.
- C. Niu, Z. Wang, G. Lu, T. M. Krupka, Y. Sun, Y. You, W. Song, H. Ran, P. Li, Y. Zheng, *Biomaterials* 2013, **34**, 2307.

ARTICLE

35. S. Mørup, *J. Magn. Magn. Mater.* 2003, **266**, 110.
36. C. W. Jung, P. Jacobs, *Magn. Reson. Imaging* 1995, **13**, 661.
37. J. T. Rosenberg, J. M. Kogot, D. D. Lovingood, G. F. Strouse, S. C. Grant, *Magn. Reson. Med.* 2010, **64**, 871.
38. A. Göpferich, *Biomaterials* 1996, **17**, 103.
39. M. L. Forrest, C.-Y. Won, A. W. Malick, G. S. Kwon, *J. Control. Release* 2006, **110**, 370.
40. A. Budhian, S. J. Siegel, K. I. Winey, *J. Microencapsulation* 2005, **22**, 773.
41. N. Ubrich, P. Bouillot, C. Pellerin, M. Hoffman, P. Maincent, *J. Control. Release* 2004, **97**, 291.
42. Y. Lee, S. Y. Park, H. Mok, T. G. Park, *Bioconj. Chem.* 2007, **19**, 525.
43. C.-H. Lee, S.-H. Cheng, Y.-J. Wang, Y.-C. Chen, N.-T. Chen, J. Souris, C.-T. Chen, C.-Y. Mou, C.-S. Yang, L.-W. Lo, *Adv. Funct. Mater.* 2009, **19**, 215.
44. C. Zheng, M. Zheng, P. Gong, D. Jia, P. Zhang, B. Shi, Z. Sheng, Y. Ma, L. Cai, *Biomaterials* 2012, **33**, 5603.
45. A. Cambon, A. Rey-Rico, D. Mistry, J. Brea, M. I. Loza, D. Attwood, S. Barbosa, C. Alvarez-Lorenzo, A. Concheiro, P. Taboada, V. Mosquera, *Int. J. Pharm.* 2013, **445**, 47.
46. J. Merloo, G. L. Kaspers, J. Cloos, in *Cancer Cell Culture*. Ed. I. A. Cree; Humana Press, New York, 2011, Vol. 731, p.237.
47. T. Minko, P. Kopeckova, V. Pozharov, J. Kopecek, *J. Control. Release* 1998, **54**, 223.
48. H. S. Yoo, K. H. Lee, J. E. Oh, T. G. Park, *J. Control. Release* 2000, **68**, 419.
49. D. Hanahan, R. A. Weinberg. *Cell* 2011, **144**, 646.
50. T. S. Hauck, T. L. Jennings, T. Yatsenko, J. C. Kumaradas, W. C. W. Chan, *Adv. Mater.* 2008, **20**, 3832.
51. A. K. Silva, E. L. Silva, A. S. Carrico, E. S. Egitto, *Curr. Pharm. Des.* 2007, **13**, 1179.
52. H. Oliveira, E. Perez-Andres, J. Thevenot, O. Sandre, E. Berra, S. Lecommandoux, *J. Control. Release* 2013, **169**, 165.
53. Saxena, M. Sadoqi, J. Shao, *Int. J. Pharm.* 2006, **308**, 200.
54. Z. Poon, J. B. Lee, S. W. Morton, P. T. Hammond, *Nano Lett.* 2011, **11**, 2096.
55. R. B. Dickson, S. E. Bates, M. E. McManaway, M. E. Lippman, *Cancer Res.* 1986, **46**, 1707.
56. Z. Mi, H. Guo, M. B. Russell, Y. Liu, B. A. Sullenger, P. C. Kuo, *Mol. Ther* 2008, **17**, 153.
57. J. Kreuter, P. Ramge, V. Petrov, S. Hamm, S. E. Gelperina, B. Engelhardt, R. Alyautdin, H. von Briesen, D. J. Begley, *Pharm. Res.* 2003, **20**, 409.V.
58. S. Gelperina, O. Maksimenko, A. Khalansky, L. Vanchugova, E. Shipulo, K. Abbasova, R. Berdiev, S. Wohlfart, N. Chepurnova, J. Kreuter, *Eur. J. Pharm. Biopharm.* 2010, **74**, 157.
59. S. Wohlfart, A. S. Khalansky, S. Gelperina, O. Maksimenko, C. Bernreuther, M. Glatzel, J. Kreuter, *PLoS One* 2011, **6**, e19121.
60. T. K. Jain, M. A. Morales, S. K. Sahoo, D. L. Leslie-Pelecky, V. Labhasetwar, *Mol. Pharm.* 2005, **2**, 194.
61. R. Manchanda, A. Fernandez-Fernandez, A. Nagesetti, A. J. McGoron, *Colloids Surfaces B: Biointerfaces* 2010, **75**, 260.
62. P. Iglesias, M. Fraga, J. A. Costoya, *Eur. J. Cancer* 2013, **49**, 264.